

Conserved Mode of Interaction between Yeast Bro1 Family V Domains and YP(X)nL Motif-Containing Target Proteins

| | |
|-------|--|
| メタデータ | 言語: eng 出版者: 公開日: 2015-11-17 キーワード (Ja): キーワード (En): 作成者: Kimura, Yoko, Tanigawa, Mirai, Kawawaki, Junko, Takagi, Kenji, Mizushima, Tsunehiro, Maeda, Tatsuya, Tanaka, Keiji メールアドレス: 所属: |
| URL | http://hdl.handle.net/10297/9265 |

20 **Abstract**

21 Yeast Bro1 and Rim20 belong to a family of proteins, which possess a common architecture
22 of Bro1- and V-domains. Alix and HD-PTP, mammalian Bro1 family proteins, bind YP(X)nL (n = 1
23 ~ 3) motifs in their target proteins through their V domains. In Alix, the Phe residue, which is located
24 in the hydrophobic groove of the V domain, is critical for binding to the YP(X)nL motif. Although
25 the overall sequences are not highly conserved between mammalian and yeast V domains, we show
26 that the conserved Phe residue in the yeast Bro1 V domain is important for binding to its
27 YP(X)nL-containing target protein, Rfu1. Furthermore, we show that Rim20 binds to its target
28 protein Rim101 through the interaction between the V domain of Rim20 and the YPIKL motif of
29 Rim101. The mutation of either the critical Phe residue in the Rim20 V domain or the YPIKL motif
30 of Rim101 affected the Rim20-mediated processing of Rim101. These results suggest that the
31 interactions between V domains and YP(X)nL motif-containing proteins are conserved from yeast to
32 mammalian cells. Moreover, the specificities of each V domain to their target protein suggest that
33 unidentified elements determine the binding specificity.

34

35 **Introduction**

36 Yeast Bro1 belongs to a family of related proteins that share a common architecture
37 comprising an N-terminal Bro1 homology domain and a following V domain (Fig. 1A). Bro1/Vps31
38 was originally isolated as one of the vacuolar protein targeting mutants and later classified as class E
39 vps mutants (1, 2). Bro1 is reported to function as an accessory factor for Endosomal Sorting
40 Complex Required for Transport (ESCRT) apparatus in the multivesicular bodies (MVB) pathway (3,
41 4). The ESCRT apparatus, which comprises four complexes (ESCRT-0, I, II, and III), is responsible
42 for the sorting of ubiquitinated membrane proteins into MVBs for degradation in the
43 lysosome/vacuole (5). Bro1 is directed to endosomes by the association of the Bro1 domain with
44 ESCRT-III subunit Snf7 (6), and was reported to regulate the membrane-scission activity of

45 ESCRT-III (7). Moreover, Bro1 binds to the deubiquitinating enzyme Doa4 through its C-terminus
46 region, recruits Doa4 to endosomes, and activates Doa4 (8, 9). Doa4 plays a role in the recovery of
47 ubiquitins from ubiquitinated cargoes just prior to the invagination of the cargo protein-enriched
48 membranes; therefore, it maintains cellular ubiquitin homeostasis in yeast (10). Intriguingly, we
49 revealed that Bro1 also binds to Rfu1 (a regulator for free ubiquitin chains) through its V domain and
50 recruits Rfu1 to endosomes (11). Rfu1 also has a function to maintain ubiquitin homeostasis by
51 inhibiting Doa4 activity (12). Bro1 has an additional region called the Pro-rich region (PRR), which
52 was reported to bind Rsp5, a major ubiquitin ligase for ubiquitinating cargo proteins (13).

53 Rim20, another Bro1 family protein in yeast, functions in the pH-responsive pathway (14,
54 15). The pathway has been intensively studied in the fungi *Aspergillus nidulans* and the yeast
55 *Saccharomyces cerevisiae* (16). In this pathway, Rim101, a transcription factor, is processed through
56 the proteolytic removal of its C-terminal region in response to alkaline pH. The processed Rim101
57 then regulates the expression of alkaline-responsive genes, resulting in the adaptation to alkaline
58 conditions (17). During this activation process, Rim20 is required for the proteolytic cleavage of
59 Rim101 along with other factors such as Rim13, Rim9, Rim21, Dfg16, Rim8, and several ESCRT-I,
60 -II, and -III factors (18-20). Rim20 appears to function as an adaptor by directly binding to Rim101
61 and several ESCRT components such as Snf7 (18, 19). Recently, it was reported that the events of
62 the Rim101 pathway, after alkaline conditions, occurred on the plasma membrane (21, 22).

63 The mammalian Bro1 homolog, apoptosis-linked gene 2 interacting protein X (Alix),
64 functions in ESCRT-mediated budding of enveloped viruses and membrane abscission in cytokinesis
65 (3, 5). During the process of virus budding, cellular ESCRT machineries are hijacked by the viruses
66 to facilitate their release from the cell membrane. Like Bro1, Alix has three main domains, Bro1, V,
67 and PRR. The PRR of Alix was shown to directly bind multiple proteins such as the Tsg101 (yeast
68 Vps23) or CEP55 (23, 24). In addition, PRR keeps Alix in an autoinhibited conformation (25, 26).
69 Although Alix has not been reported to function in the sorting of ubiquitinated cargoes such as the

70 EGF Receptor, His-domain protein tyrosine phosphatase (HD-PTP), another member of Bro1 family
71 proteins is required for EGF receptor sorting to the MVB (27).

72 The Alix V domain is about 320 amino acids (aa) long, forming the structure of two
73 trihelical bundles taking the shape of the letter V. It has been studied extensively for its interaction
74 with YP(X)nL motif-containing viral and cellular proteins (28, 29). The Alix V domain binds to the
75 YP(X)nL motif-containing late domains of retrovirus such as HIV-1, equine infectious anemia virus
76 (EIAV), and Ebola, and appears to play an important role in virus budding (30, 31). A hydrophobic
77 pocket on the second arm of Alix V was identified as a region for binding to the YP(X)nL motif
78 peptide (28, 29). Particularly, the Phe residue in the pocket plays a critical role in the interaction with
79 YP(X)nL motif, and F676D is an inactivation mutation of Alix V in binding. As for cellular proteins,
80 Alix V was shown to bind to the YPX(3)L motif of G-protein coupled receptor, protease-activated
81 receptor 1 (PAR1), to mediate the ubiquitin-independent sorting of PAR1 (32). In yeast, Bro1 and
82 Rim20 V domains were shown to have a very similar structure to the Alix V domain, albeit they have
83 a low sequence similarity(33). Recently, the V domains of Alix, HD-PTP, Bro1, and Rim20 are
84 shown to bind to ubiquitins, particularly to K63-linked ubiquitin chains (33-35), leading to the
85 proposal that V domains are ubiquitin receptors. The ubiquitin binding regions within the V domains
86 were reported to be different from the YP(X)nL binding region.

87 Because amino acid sequences are not highly conserved between Alix and yeast V domains
88 (11–13% amino acid identity for Alix and Bro1 V domains, Sup Fig. 1), the interaction of the yeast V
89 domain with a YP(X)nL motif-containing protein is overlooked (33). Recently, we showed a direct
90 interaction between a region containing the YPEL motif of Rfu1 and the V domain of Bro1 (11). In
91 this study, we observed that a region containing a critical Phe residue that is reported to bind to
92 YP(X)nL motif of the target proteins in Alix is relatively conserved in the V domains of Alix,
93 HD-PTP, Bro1, and Rim20 (Fig. 1). Therefore, we tested whether the yeast V domain's interaction
94 with YP(X)nL motif-containing target proteins could be analogous to mammalian V domains. We

95 examined the interactions between the Bro1 V–Rfu1 and Rim20 V–Rim101 by focusing on the
96 conserved Phe residue in the V domains of Bro1 and Rim20.

97

98 Experimental Procedures

99 **Media.** Yeast strains were grown in YPAD medium (1% yeast extract, 2% Bacto–Peptone, 2%
100 glucose, and 0.002% adenine), in synthetic complete medium (SD; 0.67% yeast nitrogen base and
101 2% glucose supplemented with amino acids) or synthetic casamino medium (SC; 0.67% yeast
102 nitrogen base, 2% glucose, and 0.5% casamino acids). If necessary, tryptophan, uracil, or adenine
103 was added. For microscopy studies, 0.02% adenine was added.

104

105 **Yeast strains and plasmids.** A list of the yeast strains and plasmids used in this study are provided
106 in Sup. Tables 1 and 2, respectively. Plasmid pGST2-Alix (360–702) was obtained from Addgene.
107 Plasmid expressing N-terminally myc-tagged Rim20 under the control of a *RIM20* promoter was
108 created as follows. Two kinds of DNA fragments, F and B, were amplified using a *RIM20* plasmid as
109 a template and two sets of primers, RIM20–up875–BamHI,
110 AATTAGGATCCACGTTGTATATTTTCAATCTGGAAAGTAA and RIM20–BtsI-AS,
111 GTTCACTCATGTCACACTGCCTGGATCTCC; RIM20–BtsI–Myc-sense,
112 AATTGCAGTGTGACATGGAACAAAAGCTTATTTCTGAAGAAGACTTGATGAGTGAAGTGC
113 TTGCCATTCC and RIM20–Down–XhoI-AS,
114 AATTCTCGAGCTGTTGTCTAAAGGCGAAACTACGATGAAG, respectively. The obtained F and
115 B fragments were cut with BamHI–BtsI and BtsI–XhoI, respectively. The two fragments were ligated
116 to the BamHI–XhoI vector portion of pRS315.

117

118 **Immunoblotting.** Preparation of whole-cell extracts and immunoblot analysis were performed as
119 previously described (36). In western blotting, blots were incubated with a mouse anti-GFP

120 monoclonal antibody (Roche), an anti-HA antibody (HA.11, COVANCE), or an anti-yeast PGK
121 antibody (Molecular Probes, Eugene, OR), followed by horseradish peroxidase (HRP)-conjugated
122 anti-mouse IgG (#NA931V, Amersham) and then visualized using an ECL-plus reagent (Amersham).
123 To detect GST, an HRP-conjugated anti-GST antibody (Wako) was used. A rabbit anti-yeast Bro1
124 antibody was described previously (11).

125

126 **Recombinant protein purification.** MBP-Rfu1 and MBP-fusions of the Rfu1 mutants were purified
127 as previously described (12). Recombinant GST, GST–Bro1, or the various GST–Bro1 mutants were
128 purified using glutathione chromatography as recommended by the manufacturer (GE Healthcare).
129 Recombinant proteins were eluted with 20 mM glutathione, 50 mM Tris HCl (pH 8.0), and 2 mM
130 DTT; dialyzed against 50 mM Tris HCl (pH 7.5), 100 mM NaCl, and 10% glycerol; and then stored
131 at –80°C.

132

133 ***In vitro* binding between various MBP-fused proteins and GST-fused proteins.** Binding
134 experiments were performed as previously described (11).

135

136 **Microscopy.** FM4-64 (Molecular Probes, Inc.) staining was performed as previously described (37).
137 Cells were imaged at room temperature using a confocal microscope (LSM780; Carl Zeiss) equipped
138 with an α Plan-Apochromat 100 \times oil objective lens. Images were processed using the LSM image
139 browser, and the brightness and contrast were adjusted using Adobe Photoshop CS4.

140

141 **Detection of HA–Rim101.** Logarithmically growing cells in SC-Ura Leu or SC-Ura (pH 4.0)
142 medium were harvested by centrifugation and re-suspended in the same medium, SC-Ura Leu or
143 SC-Ura (pH 8.0). After incubating for 20 min at 30°C, trichloroacetic acid (TCA) was added to make
144 a final concentration of 6% and the mixture was kept on ice for 20 min. Cells collected by

145 centrifugation were suspended in a urea buffer (50 mM Tris–HCl pH 7.5, 5 mM EDTA, 6 M urea,
146 1% SDS, 50 mM NaF, 1 mM phenylmethylsulfonyl fluoride) and were disrupted by vortexing with
147 glass beads. Obtained cell lysates were cleared by centrifugation and the total protein concentrations
148 were determined using the DC protein assay (Bio-Rad, Richmond, CA). The cell lysates were
149 incubated with a Laemmli SDS sample buffer at 65°C for 15 min and were subjected to SDS-PAGE
150 and western blotting. To detect HA-tagged Rim101 and Myc-tagged Rim20, membranes were
151 blocked with 1% skimmed milk and then immunoblotted with an anti-HA antibody (12CA5) or an
152 anti-myc antibody (9E10), respectively. The membranes were then treated with an anti-mouse IgG
153 secondary antibody conjugated with horseradish peroxidase (NA931; GE Healthcare) and developed
154 with ECL Prime (GE Healthcare). To detect actin, an anti-actin monoclonal antibody (C4; ICN,
155 Aurora, OH) and IRDye-conjugated anti-mouse IgG antibody (Rockland, Gilbertsville, PA) were
156 used. The signals were detected by using the infrared imaging system Odyssey (LICOR, Lincoln,
157 NE).

158

159 Results

160 **Effect of Phe687 of Bro1 on the interaction with Rfu1.** We noticed that the Phe residue and the
161 following Tyr as well as several neighboring residues were conserved around this region in Bro1 and
162 Rim20 V domains of *S. cerevisiae* and the Bro1 V domain of *Naumovozyma castellii* whose crystal
163 structure was resolved (33) (Fig. 1B). This suggests that this region in the V domains of Bro1 and
164 Rim20 may have similar functions as the Alix V domain.

165 In Bro1, Phe687 is the corresponding Phe residue. First, we examined the effect of the Phe
166 687 mutation in the Bro1 V domain for the binding of Rfu1 *in vitro* (Fig. 2A). In the previous work,
167 we found that recombinant MBP–Rfu1 specifically bound to the recombinant GST-fused Bro1 V
168 domain (11). We observed that the binding activity of GST–Bro1-V (F687A) to MBP–Rfu1 was
169 drastically reduced (Fig. 2A). Additionally, we examined the binding ability of mutants whose

170 mutations were closely located to F687; F677A, D680A, and L681A. The binding of Bro1 V
171 (F677A) was moderately reduced, but not as much as that of F687A Bro1 V and D680A. L681A
172 double mutations had no effects.

173 Next, we investigated whether the Bro1 F687 residue functioned in the interaction with
174 Rfu1 *in vivo*. Immunoprecipitation analysis, using lysates from cells expressing Rfu1-3 × Flag plus
175 myc-tagged Bro1 or myc-tagged Bro1 (F687A), were performed using anti-Flag. Myc-tagged Bro1,
176 but not myc-tagged Bro1 (F687A), was specifically precipitated with Rfu1-3 × Flag (Fig. 2B). These
177 results indicated that Bro1 Phe687 played a critical role in the Bro1–Rfu1 interaction both *in vitro*
178 and *in vivo*.

179 The Rfu1 localization at endosomes largely depends on Bro1; Rfu1–GFP is mainly diffusive
180 in the $\Delta bro1$ mutant, and the Rfu1 mutant in which the YPEL motif was changed to AAEL showed
181 impaired endosomal localization (11). We, therefore, examined the effect of the F687A mutation on
182 the localization of Rfu1–GFP fusions in yeast. First, we found that Bro1–GFP and Bro1
183 (F687A)–GFP were similarly observed, mainly at the class E compartments in $\Delta vps4\Delta bro1$ cells
184 (data not shown). Next, the localization of Rfu1–GFP expressed under the *RFU1* promoter was
185 examined in $\Delta rfu1\Delta vps4\Delta bro1$ cells expressing either a wild-type or F687A Bro1. Rfu1–GFP
186 fluorescence was present at foci that overlapped with FM4-64 stained class E compartments in
187 Bro1-expressing $\Delta vps4\Delta rfu1$ cells (Fig. 3A, B). In contrast, the localization of Rfu1–GFP at class E
188 compartments was reduced in Bro1 (F687A) expressing cells. The accumulation of Rfu1–GFP was
189 slightly reduced, probably due to its impaired binding to Bro1 (F687A) because a reduction in the
190 accumulation of Rfu1 was previously observed in the $\Delta bro1$ mutant (Fig. 3C) (11).

191 **Rim20 and Rim101 interaction through the V domain of Rim20 and the YPKIL motif in**
192 **Rim101.** Next, we looked for different interactions between V domains and YP(X)nL
193 motif-containing proteins. Rim20, another V-domain-containing protein, is required for Rim101p
194 processing by direct binding to Rim101 (14, 38). Xu and Mitchell showed that the C-terminus region

195 containing PEST-like sequences in Rim101 was sufficient for binding to Rim20 (14). Within the
196 C-terminus region of Rim101, there is a YPKIL motif close to the C-terminus end that matches with
197 the consensus YP(X)nL (n = 1–3) motif (39). This motif is located downstream of the cleavage site
198 of Rim101. In addition, about the C-terminal half (353–661aa) of Rim20, that corresponds to its
199 V-domain, was reported to bind to Rim101 (14).

200 To test whether the Rim101–Rim20 interaction was mediated by the Rim20’s V-domain and
201 the Rim101’s YPKIL motif, we assessed the interaction in the *in vitro* binding experiment. We made
202 recombinant MBP–Rim101-C, a fusion of MBP with the 125 aa of the C-terminal region of Rim101,
203 and checked whether MBP–Rim101-C bound to recombinant GST–Rim20 V (330–661aa) *in vitro*
204 (Fig. 4). As expected, we observed an efficient interaction between the two proteins (Fig. 4, lane 2).
205 When the conserved Rim20 Phe623 was substituted by Ala in GST-Rim20 V, the binding ability was
206 significantly lost (Fig. 4, lane 3). Moreover, we observed that the interaction between GST–Rim20V
207 and MBP–Rim101-C (Y620A, P621A), in which the YPKIL motif was changed to AAKIL, was
208 significantly lost (Fig. 4, lane 5). These results suggest that the interaction between Rim20 and
209 Rim101 is mediated by the Rim20 V domain and the YPKIL motif of Rim101, and the conserved
210 Phe in the Rim20V is critical for the interaction.

211 Next, we investigated the role of Phe623 in the Rim20 V domain by examining the
212 processing of Rim101 *in vivo* (Fig. 5). N-terminally myc-tagged or non-tagged Rim20 or Rim20
213 (F623A) were expressed in the $\Delta rim20$ mutant together with HA-tagged Rim101. Under acidic
214 conditions (pH 4), the intact full length of Rim101 is a major form; whereas, under alkaline
215 conditions (pH 8), Rim101 undergoes proteolytic processing that removes the C-terminal region of
216 Rim101 (15). As previously reported (14), the processing was defective in the $\Delta rim20$ mutant. When
217 wild-type Rim20 or myc-tagged Rim20 were introduced to the $\Delta rim20$ mutant, Rim101 processing
218 became normal. In contrast, Rim101 processing was defective in the $\Delta rim20$ mutant expressing
219 Rim20 (F623A) or myc-tagged Rim20 (F623A). We observed that the amino acid change of F623A

220 did not affect the stability of myc-Rim20 (F623A), and its level was similar to that of myc-Rim20
221 (Fig 5 A).

222 In addition, we investigated the effect of the YPKIL mutation of Rim101 on its processing
223 by expressing HA-Rim101 or HA-Rim101 (Y620A, P621A) in $\Delta rim101$ cells, and observed that
224 proteolytic processing was defective in cells expressing Rim101 (Y620A, P621A) (Fig. 5B). Because
225 the mutants in the Rim101 pathway show sensitivity to LiCl-containing medium (20, 40), LiCl
226 sensitivity was examined (Fig. 5C). Cells expressing Rim101 (Y620A, P621A) showed a marginal
227 but significant sensitivity, indicating that the active form of Rim101 was not efficiently produced
228 from Rim101 (Y620A, P621A). These results indicated that the interaction between the Rim20 V
229 domain and the YPKIL motif of Rim101 was important for their biological function.

230 **Specificity of the V domain–YP(X)nL interaction.** The V domains of Bro1 and Rim20 are
231 structurally similar; however, their physiological roles have been reported to be different. It was
232 reported that the $\Delta bro1$ mutant showed normal Rim101 processing (14), and the involvement of
233 Rim20 in MVB sorting has not been reported. We therefore suspected that there were specificities for
234 their interactions. To test the idea, we examined whether Rfu1 bound to the Rim20 V domain or
235 whether Rim101 bound to Bro1 V (Fig. 6). We observed that under the conditions that MBP–Rfu1
236 bound to Bro1 V, MBP–Rfu1 did not bind Rim20 or the Alix V domains. Similarly, MBP–Rim101-C
237 bound to Rim20 V but did not bind to Bro1-V or Alix V. These results suggest that there are more
238 unidentified determinants for the specific interaction between V domains and YPX(n)L motifs.

239

240

241 Discussion

242 In this study, we showed that the conserved Phe residue in the V domains of yeast Bro1 and Rim20
243 plays an important role in binding to the YP(X)nL-motif of their target proteins, Rfu1 and Rim101.
244 The results suggest that the yeast Bro1 and Rim20 V domains bind to their target proteins in a similar
245 way as mammalian Alix V does, indicating that V-domains are YP(X)nL-motif binding domains
246 from yeast to mammals. Therefore, results from yeast Bro1 family V domain studies will not only
247 contribute to our understanding of the cellular events in yeast, but may also be informative in our
248 understanding of the interactions between mammalian Bro1 family proteins and their
249 YP(X)nL-containing target proteins such as virus proteins.

250 In addition, we showed that there are specificities of each V domain with its target protein;
251 the C-terminal region of Rim101 specifically binds to the Rim20 V domain, but not to the Bro1 and
252 Alix V domains. Likewise, Rfu1 only binds to Bro1 V but not to Rim20 V domains in our *in vitro*
253 assay. These results suggest that there must be more unidentified sequence or structural determinants
254 of the interaction between V domains and their cognate YP(X)nL motif-containing partners (e.g.,
255 particular sequence or structures). Indeed, there are many proteins that possess YP(X)nL motifs in a
256 cell, but only a subset of them seem to bind to the V domains. For example, the YPFL motif of Doa4
257 does not bind to the Bro1 V domain, instead this motif binds to the C-terminal region of Bro1 (8).
258 Although we do not have any hints for the determinants, an intensive mutagenesis approach may
259 give us a clue to understand the nature of the specificity. In any case, a structural analysis of the Bro1
260 V domain-YPEL peptide or the Rim20 V domain-YPKIL peptide will be needed to define the precise
261 mechanism of the interaction. Moreover, finding more Bro1 V domain-binding proteins and
262 comparing their sequences or structures with those of Rfu1 or Alix V binding proteins may give us
263 some ideas of the specificities.

264 Bro1 is required for Rfu1 to function at endosomes (11). Rfu1 is involved in ubiquitin
265 homeostasis because in $\Delta rfu1$ cells, monomer ubiquitin is increased and unanchored ubiquitin chains

266 or small ubiquitin species decreased (11, 12). We expected that $\Delta bro1$ cells expressing Bro1 (F687A)
267 would show a similar ubiquitin profile to that of the $\Delta rfu1$ mutant, but they did not show obvious
268 aberrant profiles (data not shown). The reason was unknown, but it may be that the residual binding
269 of Rfu1 to Bro1 (F687A) *in vivo* is enough to support ubiquitin homeostasis, although other
270 possibilities cannot be excluded.

271 Alix has been reported to have a flexible structure (25, 26). The PRR was reported to fold
272 back and inhibit V domain binding to viral proteins. The V domain appears to take a closed
273 conformation in the presence of PRR and an open conformation in the absence of the PRR. Alix was
274 also reported to have a dimer structure via its V domain (41). Moreover, binding of ubiquitins to Alix
275 V was shown to induce oligomerisation of the V domain (35). Thus, conformational change of Bro1
276 family proteins as a whole as well as its V domain seem to be regulated in complex ways in a cell,
277 and the Bro1 family studies using tractable yeasts would be suitable to reveal such complex
278 mechanisms.

279

280

281 Acknowledgements

282 This work was supported by JSPS KAKENHI Grant Numbers 26440070 (to Y. K.) and 25291042 (to
283 T. M.).

284

285 Figure 1. Bro1 family proteins

286 A. Schematic organization of Bro1, Rim20, Alix, and HD-PTP. Bro1, V domain, and PRR (proline
287 rich region) are indicated. PTP, phosphatase domain. B. Conservation of putative YP(X)nL binding
288 regions of the V domains of *Saccharomyces cerevisiae* (sc) Bro1, *Naumovozyma castellii* (nc) Bro1,
289 Rim20, human (hs) Alix, and HD-PTP. Alignments of scBro1 vs. ncBro1, scRim20 vs. Alix, and
290 HD-PTP vs. Alix were generated by Clustal W. Alignments of nsBro1 and hsAlix were made by

291 structural comparisons using DaliLite. These alignments were then assembled. Arrow indicates the
292 critical Phe residue in the Alix V domain and the corresponding Phe in other Bro1 family proteins.

293

294 Figure 2. Impaired binding of Bro1 (F687A) to Rfu1

295 A. Impaired binding of Bro1 V (F687A) to MBP-Rfu1 *in vitro*. MBP or MBP-Rfu1 were mixed
296 with GST, GST-Bro1 V, or the noted GST-Bro1 V mutants and the proteins were isolated with
297 amylose resin. Samples were examined by immunoblot analysis using anti-GST (top panel) and
298 anti-MBP antibodies (bottom panel). B. Impaired association of Bro1 (F687A) to Rfu1-3 × Flag *in*
299 *vivo*. Lysates of *Δbro1* cells (lane 1), or *Δbro1 RFU1-3xF* cells harboring a plasmid expressing
300 C-terminally myc-tagged Bro1 or Bro1 (F687A) (lanes 2 and 3) were immunoprecipitated with
301 anti-Flag. The resulting immune-complexes (IP) were analyzed by immunoblot using anti-Flag and
302 anti-myc.

303

304 Figure 3. Impaired endosome localization of Rfu1-GFP in Bro1 (F687A)-expressing cells

305 A. GFP and FM4-64 fluorescence and DIC microscopy of Rfu1-GFP in *Δvps4Δrfu1Δbro1* cells
306 expressing Bro1 or Bro1 (F687A). Arrowheads indicate the class E compartments. Scale bar, 5 μm
307 for upper panels, 2 μm for lower panels. B. Quantification of Rfu1-GFP foci in A. Cells containing
308 GFP foci around the vacuolar membrane were counted (n = 50 cells in each experiment), and mean
309 values of three independent experiments are shown. Standard errors (SE) are shown as bars. C.
310 Rfu1-GFP expression as determined by the anti-GFP immunoblot analysis in (A). Anti-GFP
311 immunoblot (top), anti-Bro1 immunoblot (middle), and anti-phosphoglycerate kinase (PGK)
312 immunoblot (bottom), a control for protein loading.

313

314 Figure 4. Binding of the Rim20 V domain to the Rim101 YP(X)nL motif *in vitro*

315 MBP or MBP-Rim101-C or MBP-Rim101-C (Y620A, P621A) were incubated with GST,

316 GST–Rim20 V, or GST–Rim20-V (F623A), and the proteins were isolated with amylose resin. GST,
317 GST–Rim20V, or GST–Rim20V (F623A) are indicated by arrows. Anti-GST immunoblot for pull
318 down samples (top), anti-MBP immunoblot for pull down samples (middle), and anti-GST
319 immunoblot for input (bottom).

320

321 Figure 5. Effects of Rim101 or Rim20 mutation on HA-Rim101 processing

322 A. Effects of Rim20 (F623A) mutation on HA-Rim101 processing. HA-tagged Rim101 was
323 expressed in $\Delta rim20$ cells harboring a vector or expressing Rim20, Rim20 (F623A), myc-tagged
324 Rim20 or myc-tagged Rim20 (F623A), at the indicated pH of 4 or 8. Processed (p.f.) and
325 unprocessed forms (u.f.) of HA-Rim101 are indicated. Anti-HA immunoblot analysis (top), anti-myc
326 immunoblot for myc-tagged Rim20 or Rim20 (F623A) (middle), and anti-actin blot, used as a
327 loading control (bottom). B. Effect of HA-Rim101 (AAKIL) mutation on processing. $\Delta rim101$ cells
328 harboring a vector or plasmids expressing HA-Rim101 or HA-Rim101 (AAKIL) were tested. C. Li
329 sensitivity. Cells were diluted and spotted on SC-Ura plates and YPD containing 0.3M LiCl and
330 incubated for 3 days.

331

332 Figure 6. V domain specificity against YP(X)nL motif-containing proteins

333 MBP, MBP–Rfu1, or MBP–Rim101 were incubated with GST, GST–Bro1V, GST–Rim20 V, or
334 GST–Alix V, and the proteins were isolated with amylose resin. GST-tagged samples were examined
335 by immunoblot analysis using anti-MBP and anti-GST antibodies. Anti-GST immunoblot for
336 pull-down samples (top), GST–Rim20 V and GST–Bro1V of pull-down samples are indicated by
337 arrows. Anti-MBP immunoblot for pull down samples (middle), anti-GST immunoblot for input
338 (bottom).

339

340 References

341 1. **Robinson JS, Klionsky DJ, Banta LM, Emr SD.** 1988. Protein sorting in *Saccharomyces*

342 cerevisiae: isolation of mutants defective in the delivery and processing of multiple vacuolar
343 hydrolases. *Mol Cell Biol* **8**:4936-4948.

344 2. **Raymond CK, Howald-Stevenson I, Vater CA, Stevens TH.** 1992. Morphological classification of
345 the yeast vacuolar protein sorting mutants: evidence for a prevacuolar compartment in class E vps
346 mutants. *Mol Biol Cell* **3**:1389-1402.

347 3. **Bissig C, Gruenberg J.** 2014. ALIX and the multivesicular endosome: ALIX in Wonderland. *Trends*
348 *Cell Biol* **24**:19-25.

349 4. **Odorizzi G, Katzmann DJ, Babst M, Audhya A, Emr SD.** 2003. Bro1 is an endosome-associated
350 protein that functions in the MVB pathway in *Saccharomyces cerevisiae*. *J Cell Sci*
351 **116**:1893-1903.

352 5. **Henne WM, Buchkovich NJ, Emr SD.** 2011. The ESCRT pathway. *Dev Cell* **21**:77-91.

353 6. **Kim J, Sitaraman S, Hierro A, Beach BM, Odorizzi G, Hurley JH.** 2005. Structural basis for
354 endosomal targeting by the Bro1 domain. *Dev Cell* **8**:937-947.

355 7. **Wemmer M, Azmi I, West M, Davies B, Katzmann D, Odorizzi G.** 2011. Bro1 binding to Snf7
356 regulates ESCRT-III membrane scission activity in yeast. *J Cell Biol* **192**:295-306.

357 8. **Richter C, West M, Odorizzi G.** 2007. Dual mechanisms specify Doa4-mediated deubiquitination
358 at multivesicular bodies. *EMBO J* **26**:2454-2464.

359 9. **Luhtala N, Odorizzi G.** 2004. Bro1 coordinates deubiquitination in the multivesicular body
360 pathway by recruiting Doa4 to endosomes. *J Cell Biol* **166**:717-729.

361 10. **Swaminathan S, Amerik AY, Hochstrasser M.** 1999. The Doa4 deubiquitinating enzyme is
362 required for ubiquitin homeostasis in yeast. *Mol Biol Cell* **10**:2583-2594.

363 11. **Kimura Y, Kawawaki J, Kakiyama Y, Shimoda A, Tanaka K.** 2014. The ESCRT-III adaptor protein
364 Bro1 controls functions of regulator for free ubiquitin chains 1 (Rfu1) in ubiquitin homeostasis. *J*
365 *Biol Chem* **289**:21760-21769.

366 12. **Kimura Y, Yashiroda H, Kudo T, Koitabashi S, Murata S, Kakizuka A, Tanaka K.** 2009. An
367 inhibitor of a deubiquitinating enzyme regulates ubiquitin homeostasis. *Cell* **137**:549-559.

368 13. **Nikko E, Andre B.** 2007. Split-ubiquitin two-hybrid assay to analyze protein-protein interactions
369 at the endosome: application to *Saccharomyces cerevisiae* Bro1 interacting with ESCRT
370 complexes, the Doa4 ubiquitin hydrolase, and the Rsp5 ubiquitin ligase. *Eukaryot Cell*
371 **6**:1266-1277.

372 14. **Xu W, Mitchell AP.** 2001. Yeast PalA/AIP1/Alix homolog Rim20p associates with a PEST-like
373 region and is required for its proteolytic cleavage. *J Bacteriol* **183**:6917-6923.

374 15. **Li W, Mitchell AP.** 1997. Proteolytic activation of Rim1p, a positive regulator of yeast sporulation
375 and invasive growth. *Genetics* **145**:63-73.

376 16. **Penalva MA, Lucena-Agell D, Arst HN, Jr.** 2014. Liaison alcaline: Pals entice non-endosomal
377 ESCRTs to the plasma membrane for pH signaling. *Curr Opin Microbiol* **22**:49-59.

378 17. **Maeda T.** 2012. The signaling mechanism of ambient pH sensing and adaptation in yeast and
379 fungi. *FEBS J* **279**:1407-1413.

- 380 18. **Boysen JH, Mitchell AP.** 2006. Control of Bro1-domain protein Rim20 localization by external pH,
381 ESCRT machinery, and the *Saccharomyces cerevisiae* Rim101 pathway. *Mol Biol Cell*
382 **17**:1344-1353.
- 383 19. **Xu W, Smith FJ, Jr., Subaran R, Mitchell AP.** 2004. Multivesicular body-ESCRT components
384 function in pH response regulation in *Saccharomyces cerevisiae* and *Candida albicans*. *Mol Biol*
385 *Cell* **15**:5528-5537.
- 386 20. **Hayashi M, Fukuzawa T, Sorimachi H, Maeda T.** 2005. Constitutive activation of the
387 pH-responsive Rim101 pathway in yeast mutants defective in late steps of the MVB/ESCRT
388 pathway. *Mol Cell Biol* **25**:9478-9490.
- 389 21. **Obara K, Kihara A.** 2014. Signaling events of the Rim101 pathway occur at the plasma membrane
390 in a ubiquitination-dependent manner. *Mol Cell Biol* **34**:3525-3534.
- 391 22. **Galindo A, Calcagno-Pizarelli AM, Arst HN, Jr., Penalva MA.** 2012. An ordered pathway for the
392 assembly of fungal ESCRT-containing ambient pH signalling complexes at the plasma membrane.
393 *J Cell Sci* **125**:1784-1795.
- 394 23. **von Schwedler UK, Stuchell M, Muller B, Ward DM, Chung HY, Morita E, Wang HE, Davis T, He**
395 **GP, Cimbora DM, Scott A, Krausslich HG, Kaplan J, Morham SG, Sundquist WI.** 2003. The
396 protein network of HIV budding. *Cell* **114**:701-713.
- 397 24. **Morita E, Sandrin V, Chung HY, Morham SG, Gygi SP, Rodesch CK, Sundquist WI.** 2007. Human
398 ESCRT and ALIX proteins interact with proteins of the midbody and function in cytokinesis.
399 *EMBO J* **26**:4215-4227.
- 400 25. **Zhou X, Si J, Corvera J, Gallick GE, Kuang J.** 2010. Decoding the intrinsic mechanism that
401 prohibits ALIX interaction with ESCRT and viral proteins. *Biochem J* **432**:525-534.
- 402 26. **Zhai Q, Landesman MB, Chung HY, Dierkers A, Jeffries CM, Trewella J, Hill CP, Sundquist WI.**
403 2011. Activation of the retroviral budding factor ALIX. *J Virol* **85**:9222-9226.
- 404 27. **Doyotte A, Mironov A, McKenzie E, Woodman P.** 2008. The Bro1-related protein HD-PTP/PTPN23
405 is required for endosomal cargo sorting and multivesicular body morphogenesis. *Proc Natl Acad*
406 *Sci U S A* **105**:6308-6313.
- 407 28. **Fisher RD, Chung HY, Zhai Q, Robinson H, Sundquist WI, Hill CP.** 2007. Structural and
408 biochemical studies of ALIX/AIP1 and its role in retrovirus budding. *Cell* **128**:841-852.
- 409 29. **Lee S, Joshi A, Nagashima K, Freed EO, Hurley JH.** 2007. Structural basis for viral late-domain
410 binding to Alix. *Nat Struct Mol Biol* **14**:194-199.
- 411 30. **Han Z, Madara JJ, Liu Y, Liu W, Ruthel G, Freedman BD, Harty RN.** 2015. ALIX Rescues
412 Budding of a Double PTAP/PPEY L-Domain Deletion Mutant of Ebola VP40: A Role for ALIX in
413 Ebola Virus Egress. *J Infect Dis* doi:10.1093/infdis/jiu838.
- 414 31. **Votteler J, Sundquist WI.** 2014. Virus Budding and the ESCRT Pathway. *Cell Host Microbe*
415 **14**:232-241.
- 416 32. **Dores MR, Chen B, Lin H, Soh UJ, Paing MM, Montagne WA, Meerloo T, Trejo J.** 2012. ALIX
417 binds a YPX(3)L motif of the GPCR PAR1 and mediates ubiquitin-independent ESCRT-III/MVB

418 sorting. *J Cell Biol* **197**:407-419.

419 33. **Pashkova N, Gakhar L, Winistorfer SC, Sunshine AB, Rich M, Dunham MJ, Yu L, Piper RC.** 2013.
420 The Yeast Alix Homolog Bro1 Functions as a Ubiquitin Receptor for Protein Sorting into
421 Multivesicular Endosomes. *Dev Cell* doi:S1534-5807(13)00218-9 [pii]
422 10.1016/j.devcel.2013.04.007.

423 34. **Dowlatshahi DP, Sandrin V, Vivona S, Shaler TA, Kaiser SE, Melandri F, Sundquist WI, Kopito**
424 **RR.** 2012. ALIX Is a Lys63-Specific Polyubiquitin Binding Protein that Functions in Retrovirus
425 Budding. *Dev Cell* **23**:1247-1254.

426 35. **Keren-Kaplan T, Attali I, Estrin M, Kuo LS, Farkash E, Jerabek-Willemsen M, Blutraich N, Artzi**
427 **S, Peri A, Freed EO, Wolfson HJ, Prag G.** 2013. Structure-based in silico identification of
428 ubiquitin-binding domains provides insights into the ALIX-V:ubiquitin complex and retrovirus
429 budding. *EMBO J* **32**:538-551.

430 36. **Kimura Y, Koitabashi S, Kakizuka A, Fujita T.** 2001. Initial process of polyglutamine aggregate
431 formation in vivo. *Genes Cells* **6**:887-897.

432 37. **Vida TA, Emr SD.** 1995. A new vital stain for visualizing vacuolar membrane dynamics and
433 endocytosis in yeast. *J Cell Biol* **128**:779-792.

434 38. **Ito T, Chiba T, Ozawa R, Yoshida M, Hattori M, Sakaki Y.** 2001. A comprehensive two-hybrid
435 analysis to explore the yeast protein interactome. *Proc Natl Acad Sci U S A* **98**:4569-4574.

436 39. **Vincent O, Rainbow L, Tilburn J, Arst HN, Jr., Penalva MA.** 2003. YPXL/I is a protein interaction
437 motif recognized by aspergillus PalA and its human homologue, AIP1/Alix. *Mol Cell Biol*
438 **23**:1647-1655.

439 40. **Lamb TM, Xu W, Diamond A, Mitchell AP.** 2001. Alkaline response genes of *Saccharomyces*
440 *cerevisiae* and their relationship to the RIM101 pathway. *J Biol Chem* **276**:1850-1856.

441 41. **Pires R, Hartlieb B, Signor L, Schoehn G, Lata S, Roessle M, Moriscot C, Popov S, Hinz A, Jamin**
442 **M, Boyer V, Sadoul R, Forest E, Svergun DI, Gottlinger HG, Weissenhorn W.** 2009. A
443 crescent-shaped ALIX dimer targets ESCRT-III CHMP4 filaments. *Structure* **17**:843-856.

444

445

Figure 1

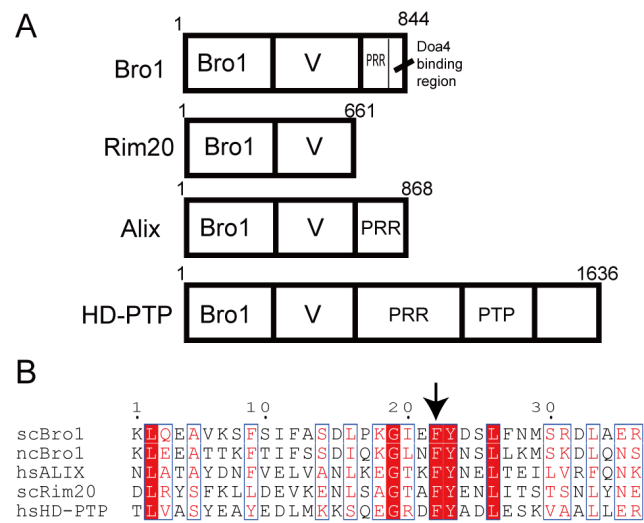


Figure 2

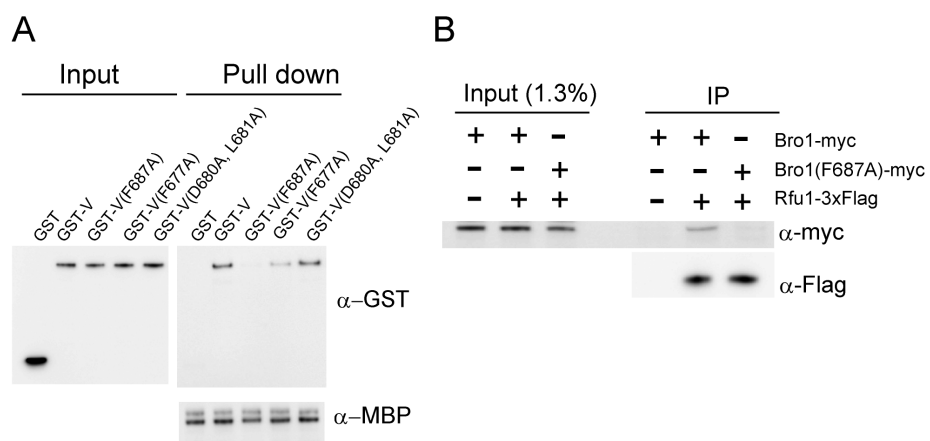


Figure 3

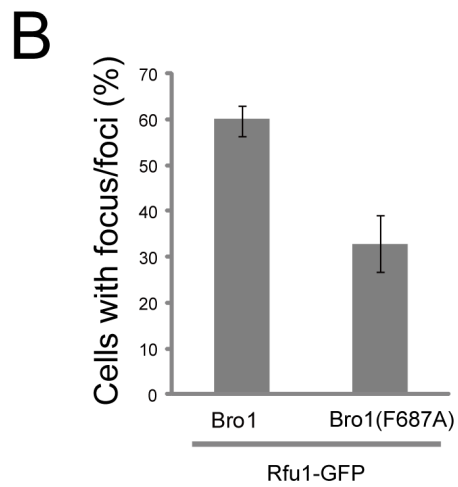
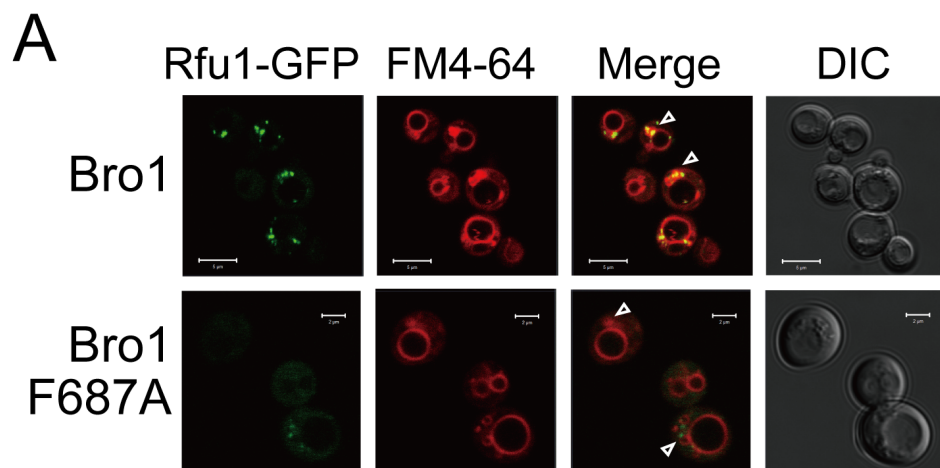


Figure 4

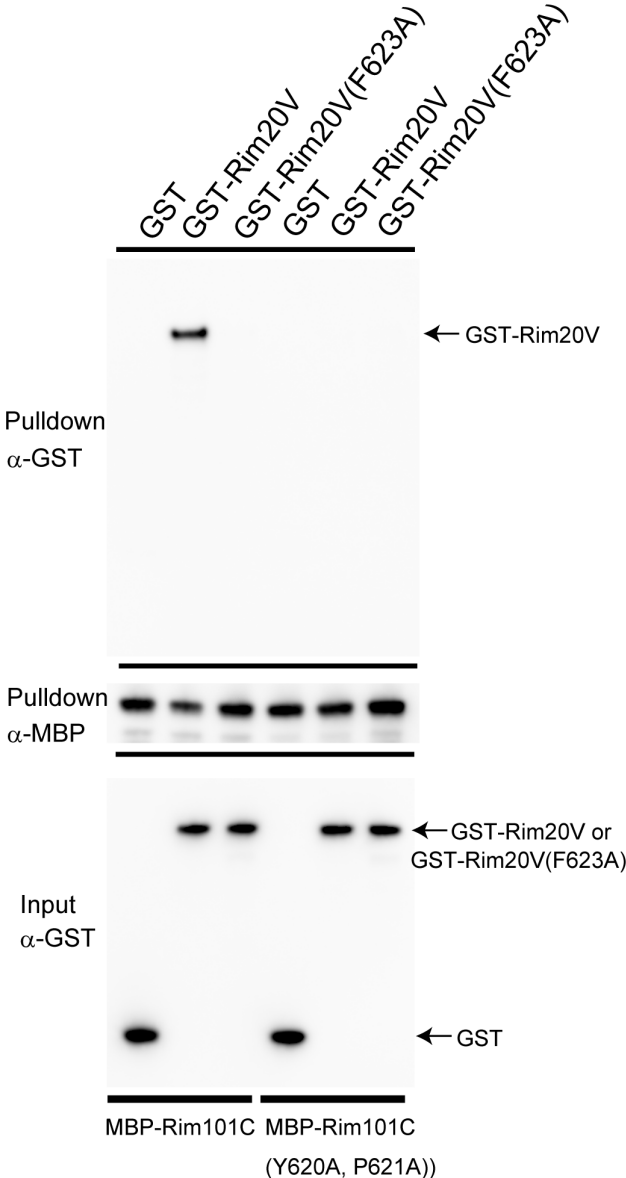


Figure 5

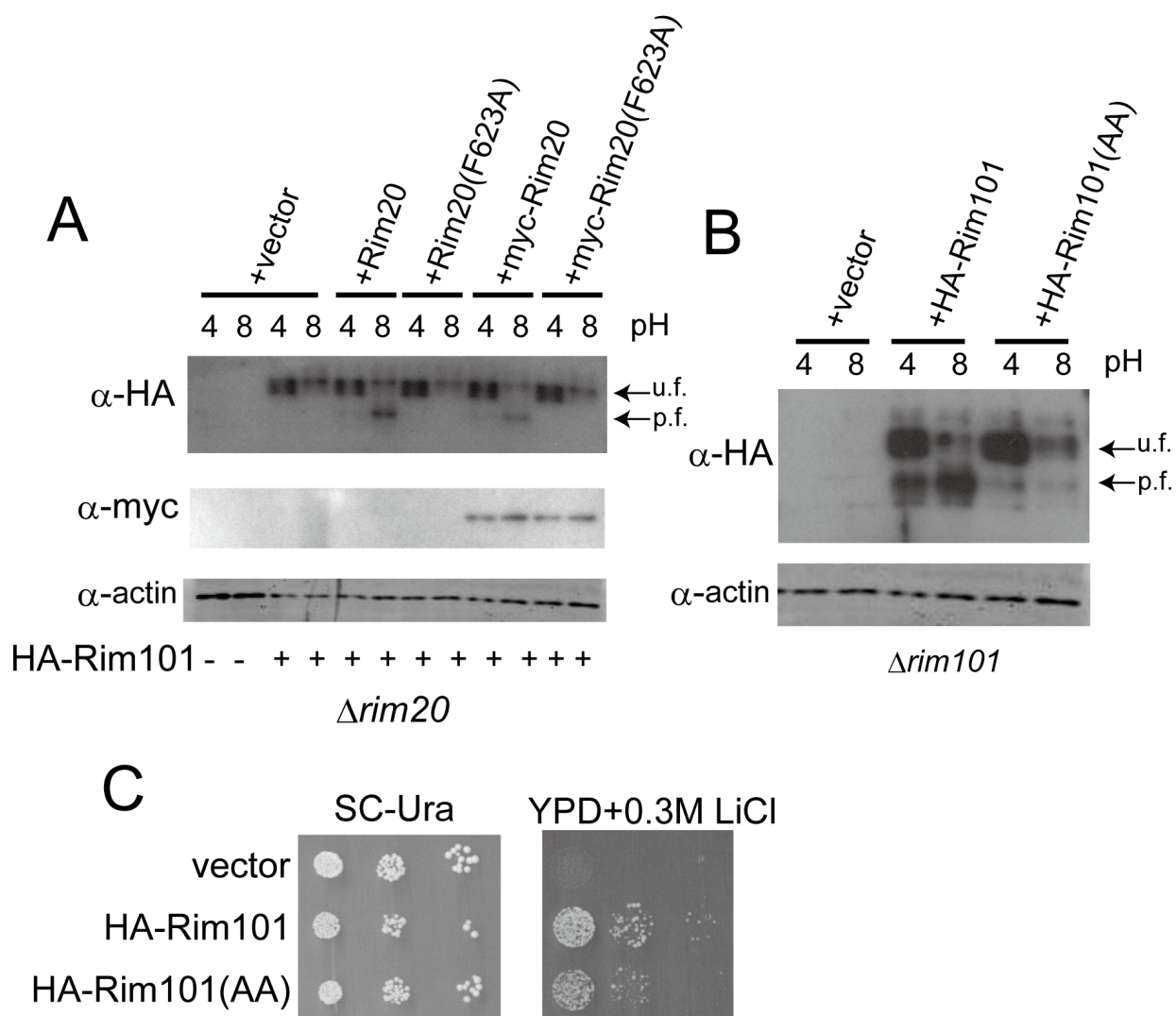
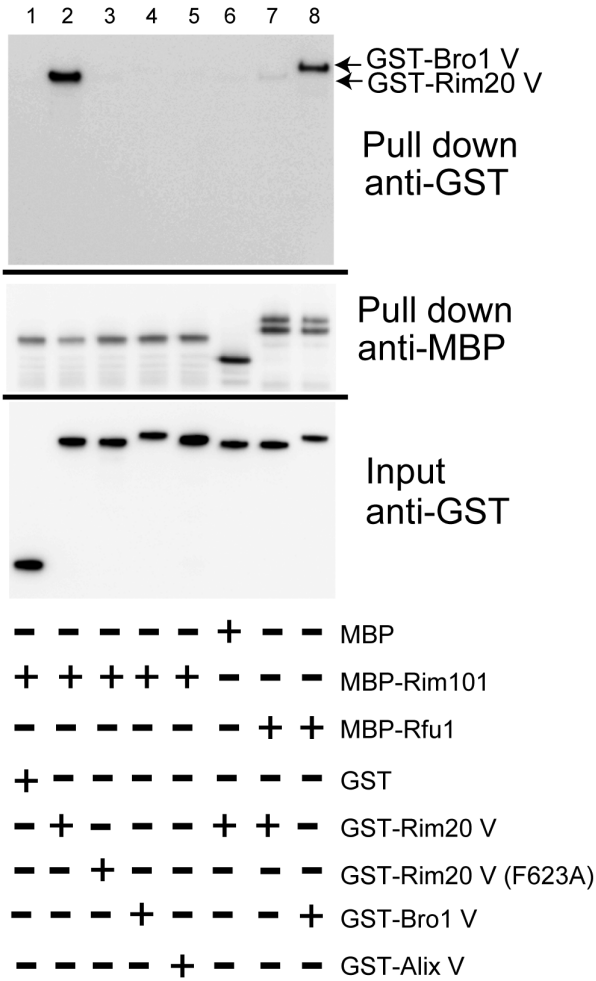


Figure 6



Supplementary Table 1. Strains used in this study

| Name | Genotype | Source/Reference |
|---------------------|---|---------------------|
| W303 | MAT α ade2-1 can1-100 his3-12,16 leu2-3,112 trp1-1 ura3-1 | Rothstein |
| Y795 | W303 α , Δ rfu1::KanMX Δ vps4::LEU2 | Kimura et al., 2014 |
| Y1009 | W303 α ; RFU1-3xFLAG::RFU1 | This study |
| Y1119 | W303 α ; RFU1-3xFLAG::RFU1, Δ bro1::HIS3 | This study |
| Y1118 | W303 α , Δ rfu1::KanMX Δ vps4::LEU2, Δ bro1::HIS3 | This study |
| Y1140 | W303 α ; Δ bro1::HIS3 | This study |
| rim101 Δ 101 | MAT α ura3-52 leu2 Δ 1 his3 Δ l200 rim101::HIS3 | This study |
| FM201 | MAT α ura3-52 leu2 Δ 1 his3 Δ 200 trp1 Δ 63 rim20::HIS3 | Hayashi et al, 2005 |

Supplementary Table S2 Plasmids used in this study

| Plasmids | Name | Proteins expressed | Characteristics | Source/References |
|----------|----------------------------------|----------------------------------|-----------------|-----------------------|
| pGCU10 | GAL1p-GFP-tADH1 | GFP | URA3, CEN | Kimata et al., (1997) |
| E798 | YCplac22-RFU1p-RFU1-GFP | Rfu1-GFP | TRP1, CEN | This study |
| E744 | pRFU1p-RFU1(1-200)-GFP | RFU1(1-200)-GFP | URA3, CEN | This study |
| pMALP2X | MBP | MBP | | |
| E382 | MBP-Rfu1(1-200) | MBP-Rfu1(1-200) | | Kimura et al., (2009) |
| E827 | MBP-RIM101(501-625) | MBP-Rim101(501-625) | | This study |
| | MBP-RIM101(501-625,Y620A, P621A) | MBP-Rim101(501-625,Y620A, P621A) | | This study |
| pGEX4T-3 | | GST | | GE |
| E779 | pGEX-Bro1-V Comp | GST-Bro1-V (361-720) | | Kimura et al., (2014) |
| E831 | pGEX-Bro1-V Comp(F687A) | GST-Bro1-V (361-720)F687A | | This study |
| E829 | pGEX-Bro1-V Comp(F677A) | GST-Bro1-V (361-720)F677A | | This study |
| E828 | pGEX-Bro1-V Comp(D680A, L681A) | GST-Bro1-V (361-720)D680A, L681A | | This study |
| E838 | pGEX-Rim20 V | GST-Rim20-V(330-661) | | This study |
| E842 | pGEX-Rim20 V(F623A) | GST-Rim20 V(330-661, F623A) | | this study |
| | pGST2-Alix (360-702) | GST-Alix V(360-702) | | Addgene |
| E813 | pRS316-BRO1 | Bro1 | URA3, CEN | This study |
| E837 | pRS316-BRO1(F687A) | Bro1(F687A) | URA3, CEN | this study |
| E846 | pRS316-BRO1myc | Bro1-myc | URA3, CEN | This study |
| E851 | pRS316-BRO1(F687A)myc | Bro1(F687A)-myc | URA3, CEN | This study |
| E847 | pRS315-RIM20 | Rim20 | LEU2, CEN | This study |
| E854 | pRS315-RIM20(F623A) | Rim20(F623A) | LEU2, CEN | This study |
| E848 | pRS315-mycRIM20 | Myc-Rim20 | LEU2, CEN | This study |
| E855 | pRS315-mycRIM20(F623A) | Myc-Rim20(F623A) | LEU2, CEN | This study |
| E860 | LRIM101m1HApRS416 | HA-Rim101 | URA3 | This study |
| E861 | pRS416-HA-RIM101(Y620A, P621A) | HA-Rim101(Y620A, P621A) | URA3 | This study |